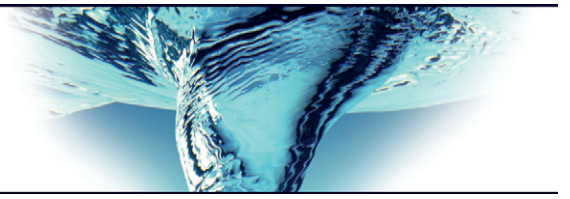
CrossMark

J. Fluid Mech. (2017), *vol.* 822, R5, doi:10.1017/jfm.2017.252



JFM RAPIDS
journals.cambridge.org/rapids

To flap or not to flap: comparison between flapping and clapping propulsions

Nathan Martin[1], **Chris Roh**[1], **Suhail Idrees**[2] **and Morteza Gharib**[1,†]

[1]Division of Engineering and Applied Science, California Institute of Technology, Pasadena, CA 91125, USA

[2]Department of Engineering, University of Cambridge, Trumpington Street, Cambridge CB2 1PZ, UK

(Received 30 November 2016; revised 11 April 2017; accepted 15 April 2017; first published online 7 June 2017)

A comparison between swimming by flapping and by periodic contractions is conducted. Swimming by flapping is approximated as a pitching plate while swimming by periodic contractions is approximated as clapping plates. A direct comparison is made between the two propulsion mechanisms by utilizing a machine that can operate in either a flapping or a clapping mode between Reynolds numbers of 1880 and 11 260 based on the average plate tip velocity and span. The average thrust generated and the average input power required per cycle are compared between cases where the total sweep angle and the total sweep time are identical. Variation of the kinematics results in a similar thrust between the two mechanisms, but a greater power is required for clapping. Variation of the flexibility results in a consistent decrease in the required power for clapping and a decrease in thrust at high flexibility. Variation of the duty cycle for clapping rigid plates results in a significant increase in thrust and a significant decrease in the required power. Overall, the results suggest that flapping propulsion is the more effective propulsion mechanism within the range of Reynolds numbers tested.

Key words: biological fluid dynamics, propulsion, swimming/flying

1. Introduction

Swimming by flapping and swimming by periodic contractions are common motions used by underwater animals. Flapping is commonly used by fish and cetaceans while periodic contractions are commonly used by jellyfish and squid. Both mechanisms of propulsion have been widely studied separately.

The flapping motion is often simplified to a plate pitching about its leading edge. Early work on this motion was conducted by Koochesfahani (1989), who showed that the oscillation frequency and sweep angle of a rigid pitching airfoil affect the

† Email address for correspondence: mgharib@caltech.edu

© Cambridge University Press 2017

https://doi.org/10.1017/jfm.2017.252 Published online by Cambridge University Press

mean velocity profile of the generated vortex street. The impact of flexibility was later investigated by Dai *et al.* (2012), who found that the thrust and efficiency of flexible pitching plates are optimized at a reduced stiffness $K = EI/(\rho U_\infty^2 s^3 c)$. of 5 and collapse onto a single curve regardless of flexibility when plotted against the Strouhal number $St = fL/U_\infty$. Here, E is the elastic modulus of the plate, I is the second moment of area of the plate, ρ is the density of the fluid, U_∞ is the free-stream velocity, c is the chord length of the plate, s is the span of the plate, f is the oscillation frequency of the plate and L is the excursion length of the tip of the tail. The impact of aspect ratio was recently investigated by Yeh & Alexeev (2016), who showed that smaller aspect ratio plates can travel greater distances for less power. The aspect ratio is defined as the span s divided by the chord length c. In summary, these works have shown that smaller aspect ratio plates have better performance, and emphasized the importance of sweep angle, frequency and flexibility.

The periodic contraction motion is often simplified to that of clapping plates. For this motion, two plates, either attached at the leading edge or separated by a small gap, pitch symmetrically in opposite directions about the centreline. The opening motion creates two strong vortices at the tips, generating negative thrust, while the closing motion expels fluid, creating a jet that generates positive thrust. These motions are similar to portions of the clap-and-fling mechanism introduced by Weis-Fogh (1973). The closing motion is similar to the clap phase of the clap-and-fling mechanism, in which two wings have come together at an edge and pitch symmetrically towards the centreline, while the opening motion is similar to the beginning of the fling phase, where two wings pitch about an edge symmetrically away from the centreline. Recent work on clapping plates was carried out by Kim, Hussain & Gharib (2013), who found that low-aspect-ratio plates generate the strongest tip vortices, probably accounting for their greater thrust coefficients. A review of the progress on the clap-and-fling mechanism was conducted by Sane (2003).

The purpose of this study is to investigate whether swimming by flapping or by periodic contractions is the more effective motion for underwater locomotion. Here, the most effective propulsion mechanism is that which generates the greatest thrust per cycle for the least power. For this comparison, the assumption is that a hypothetical animal desires the most effective mechanism and has two posterior fins at its disposal. The research question then becomes whether the animal should put both of its fins together and pitch them in the same direction (i.e. to utilize a flapping motion) or keep its fins apart and pitch them in opposite directions (i.e. to utilize a clapping motion). It should be noted that, in this scenario, the bending rigidity, which is proportional to the thickness cubed, for flapping is only twice that used during periodic contractions instead of eight times larger as the plates are not fused together. For simplicity and for a straightforward comparison between the two mechanisms, propulsion by flapping is approximated as a plate pitching about its leading edge while propulsion by periodic contractions is approximated as clapping plates which fully open and close. The propulsion mechanisms are evaluated by constructing a machine that can operate in either mode of propulsion and comparing the thrust generated and the power required per cycle between trials of equivalent kinematics, namely total sweep angle ϕ and total sweep time t_s. For example, if the plates undergoing flapping sweep out 40° in 2 s, the two plates undergoing clapping would each sweep out 20° in 2 s. The plates are manufactured with a similar height to that of the test section (i.e. to have zero aspect ratio) for the greatest performance (Yeh & Alexeev 2016). All tests are conducted without an imposed free stream to investigate the infinite-Strouhal-number limit and started from quiescent flow.

https://doi.org/10.1017/jfm.2017.252 Published online by Cambridge University Press

The machine operates between Reynolds numbers ($Re = Us/\nu$) of 1880 and 11 260, further discussed in § 2. Here, U is the average tip velocity of the plate, s is the span of the plate and ν is the kinematic viscosity of the fluid. An analogous Re for fish can be defined based on the average tip velocity and the length of the caudal fin while that for jellyfish can be defined based on the average tip velocity and the radius of the bell. Examples of fish that swim within this range are the *Leiostomus xanthurus*, the *Brevoortia tyrannus* and the *Clupea harengus*. This was determined by assuming that the typical caudal fin has a length that is 20 % the standard length of a fish, a sweep angle of 60° (Hunter & Zweifel 1971) and an oscillation frequency between 2 and 15 Hz (Bainbridge 1958). These values give a range of Re only as a function of the frequency and the standard length of a fish, many of which are documented by Sambilay Jr. (1990). Examples of jellyfish that swim within this range are the *Chrysaora lactea*, the *Aurelia aurita* and the *Chrysaora colorata*. This was determined by assuming that the typical bell has a total sweep angle of 20°, calculated by investigating the change in the angle between fully contracted and relaxed states using line segments connecting the apex to the bottom of the bell from images in Colin, Costello & Kordula (2006), and a contraction frequency between 0.2 and 2 Hz (Colin *et al.* 2013). Again, these values give a range of Re only as a function of the frequency and the bell radius of a jellyfish, which are documented for the specific species by Graham & Kroutil (2001), Gershwin & Collins (2002) and Morandini, Da Silveira & Jarms (2004).

2. Experimental set-up and methods

The experiments are conducted using a single machine that can operate in either flapping or clapping mode for direct comparison (figure 1*a*). The design is based around two co-axial shafts, each with one attached plate; the inner shaft is directly connected to a stepper motor while the outer shaft is allowed to rotate freely. In the clapping mode, a gearbox is enabled which drives the outer shaft in the opposite direction to the inner shaft, causing the two plates to pitch symmetrically about the centreline. In the flapping mode, the gearbox is disabled and the two plates are fixed to one another so that the outer shaft is driven with the same motion as the inner shaft. The span s and chord length c of all rectangular plates are kept constant at 0.127 m and 0.457 m respectively (figure 1*b*). The thickness h is 0.9525 mm for the baseline rigid aluminium plate and 1.016, 0.508 and 0.381 mm for the flexible polycarbonate plates; the dimensional flexural rigidities of the plates $D = Eh^3/(12(1 - \nu_p^2))$, where E is the elastic modulus of the plate and ν_p is the Poisson ratio for the plate, are 5.58, 0.247, 0.031 and 0.013 Pa m^3 respectively. Another measure of flexibility is the non-dimensional reduced stiffness $K = EI/(\rho U^2 s^3 c)$. This definition is similar to that used in Dai *et al.* (2012), except that, here, U is the average speed of the trailing edge, defined as $(\phi/t_s)s$, and the second moment of area I is calculated as $ch^3/12$. The machine is driven with a sinusoidal velocity profile by an NEMA 34 single-shaft stepper motor with a 8.474 N m holding torque controlled by a GeckoDrive 213 V at 0.18° pulse^{-1}. The pulse train is generated using a National Instruments USB-6211 DAQ board. The machine is mounted on NewWay linear air bearings to isolate the force in the thrust direction (figure 1*a*). Forces are measured using a uni-axial Interface MB-5 Mini Beam Load Cell with a maximum capacity of 22.24 N, nonlinearity of 6.672 mN and hysteresis of 4.448 mN. The load cell is connected to the front of the mechanism via a universal joint to nullify the effects of any generated moments. Torques are measured using a FUTEK rotary torque sensor with a maximum

https://doi.org/10.1017/jfm.2017.252 Published online by Cambridge University Press

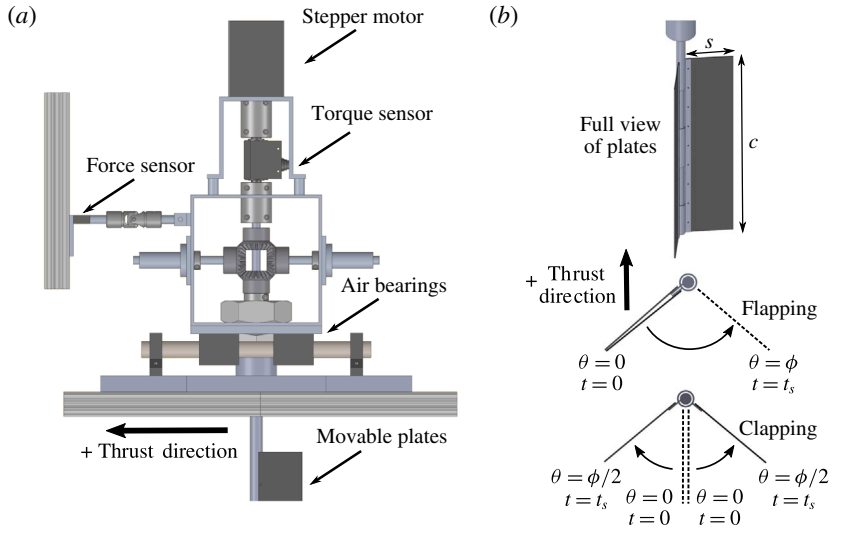


FIGURE 1. (*a*) Side view of the machine. (*b*) Definition of chord c, span s, sweep angle ϕ and sweep time t_s. In the flapping configuration, where the two plates are together, the dashed line denotes where the plates end after the first half of a cycle. In the clapping configuration, where the two plates are separated, the dashed lines denote where the plates begin the first half of the cycle. In both configurations, the arrows denote the direction of motion during the first half of the cycle, but during the second half of the cycle, the motion is reversed.

capacity of 20 N m, nonlinearity of 0.04 N m and hysteresis of 0.02 N m. The torque sensor is mounted between the stepper motor and the driven shaft. The plates are fully submerged in a free-surface water tunnel with a test section area that is 1.01 m wide and 1.83 m long with a maximum fill depth of 0.6 m. Free-surface effects are diminished by placing a Styrofoam sheet at the free surface near the top of the test plates.

Digital particle image velocimetry (DPIV, Willert & Gharib 1991) is used to investigate the flow field generated by the rigid baseline flapping and clapping plates. The flow is seeded with Potters Industries silver-coated hollow ceramic spheres (mean density 0.9 g cm^{-3} and diameter 100 μm), illuminated by an Opto Engine LLC 3 W continuous laser, creating a laser sheet along the mid-plane of the plates, and recorded using a Dantec Dynamics Nanosense MK-III at 100 frames per second. The vorticity field is computed from a phase average of three trials and used to estimate the generated thrust ($F = -F_v$) through

$$F_v = -\rho \frac{\mathrm{d}\alpha}{\mathrm{d}t} + \rho \sum_{j=1}^{N} \frac{\mathrm{d}}{\mathrm{d}t} \int_{R_j} v \, \mathrm{d}R \tag{2.1}$$

for two-dimensional flow, reproduced from Wu (1981); the flow is assumed to be two-dimensional due to the small aspect ratio of the plates. The first term is the change in the first moment of the vorticity field $\alpha \equiv \int_{R_\infty} r \times \Omega \, \mathrm{d}R$, where R_∞ is an infinite domain, r is the distance from the origin and Ω is the vorticity; this term simplifies to $\int_{R_\infty} y\omega_z \, \mathrm{d}R$ as the only force of interest, the thrust, is in the x-direction.

https://doi.org/10.1017/jfm.2017.252 Published online by Cambridge University Press

Calculation of α requires knowledge of all vortices ever created; therefore, analysis of the vorticity field is limited to the initial cycle when all vortices are within the field of view of the camera. It should be noted that $\mathrm{d}\alpha/\mathrm{d}t$ can be rewritten as $\int_{R_\infty} \omega_z(\mathrm{d}y/\mathrm{d}t) + y(\mathrm{d}\omega_z/\mathrm{d}t)\,\mathrm{d}R$ because the control volume does not change. The second term in (2.1) is the change of the velocity v inside the control volume R_j enclosing N solid bodies, which is assumed to be negligible as the plates are thin. Vortex tracking provides insight into the contribution of each vortex to the overall force.

Direct comparison between the propulsion mechanisms is restricted to cases where both the total sweep time and the total sweep angle are identical. The total sweep times t_s of interest are 3, 2 and 1 s, while the total sweep angles ϕ of interest are 40°, 60° and 80° (figure 1*b*). For the sweep time of 1 s, the only sweep angle tested is 40°, as greater accelerations are beyond the capability of the machine. These kinematics give a range of Reynolds numbers based on the average tip velocity and span of the plate, $Re = Us/\nu$, between 1880 and 11 260. Here, U is the average tip velocity of the plate, s is the span of the plate and ν is the kinematic viscosity of the fluid. Force and torque data are obtained for all combinations of sweep times and sweep angles, where each combination has at least eight trials, each with at least 10 cycles. Average forces $\overline{F}$ and torques $\overline{T}$ per cycle for a single kinematic combination are obtained by averaging the mean force and mean torque per cycle over all trials; only cycles after the flow has reached steady state are used. The average thrust, torque and power coefficients are calculated respectively as follows:

$$\overline{C}_T = \frac{\overline{F}}{\frac{1}{2}\rho U^2 A}, \quad \overline{C}_\tau = \frac{\overline{T}}{\frac{1}{2}\rho U^2 A s} \quad \text{and} \quad \overline{C}_{po} = \frac{\overline{T}\overline{\omega}}{\frac{1}{2}\rho U^2 A s/t_s}. \qquad (2.2a\text{–}c)$$

Here, $\overline{\omega} = \phi/t_s$ is the average angular velocity of the plate and $A = cs$ is the area of the plate. It should be noted that, for this choice of non-dimensionalization, $\overline{F}$ and $\overline{T}$ from flapping and clapping are divided by the same value if they share the same overall kinematics. The error bars are the standard deviations of the mean C_T and C_{po} per cycle, and although they are only plotted in one direction, they are symmetric.

3. Results and discussion

3.1. *The effect of kinematics*

The effect of kinematics is investigated by varying ϕ and t_s on flapping and clapping rigid 0.9525 mm thick aluminium plates. The average thrust coefficient $\overline{C}_T$ and the average power coefficient $\overline{C}_{po}$ are shown in figures 2(*a*) and 2(*b*) respectively; the phase average of C_T and C_τ as a function of the non-dimensional time $t^* = t/2t_s$ during the initial cycle from three trials for $\phi = 60°$ and $t_s = 2$ s is shown in figure 3, illustrating the typical behaviour and for comparison with DPIV results in § 3.2. The opening phase of clapping propulsion corresponds to the first half of the cycle while the closing phase corresponds to the second half of the cycle. The minimum reduced stiffness K of a single plate is 308.1 at a 40° sweep angle and a 1 s sweep time, meaning that the plates are effectively rigid with respect to the flow for all kinematic sets. Comparison of $\overline{C}_{po}$ between flapping and clapping propulsion, denoted by the black and grey bars respectively, for all kinematic sets shows that clapping propulsion requires on average 3.87 times the power required for flapping propulsion. This can be understood conceptually by considering the volumetric flow rate through a plane bounded by and moving with the trailing edge of each clapping plate. Near the end of the closing phase, the area approaches zero, so the velocity must approach infinity;

https://doi.org/10.1017/jfm.2017.252 Published online by Cambridge University Press

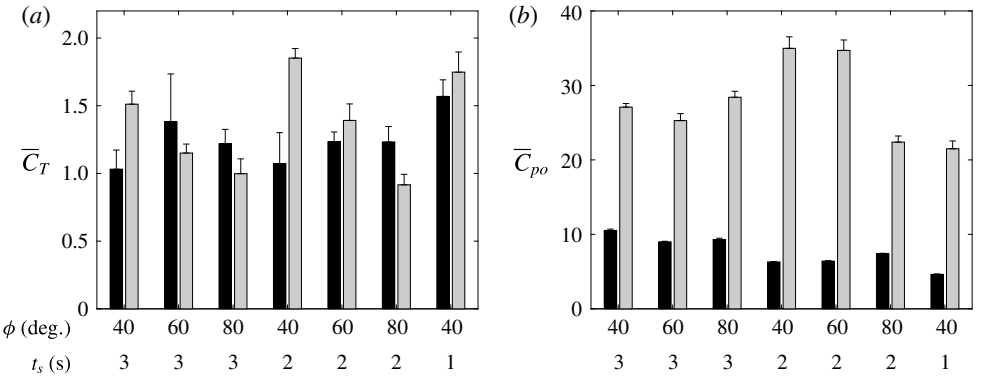


FIGURE 2. Average thrust coefficient $\overline{C}_T$ (*a*) and power coefficient $\overline{C}_{po}$ (*b*) for the baseline rigid aluminium plates as a function of plate kinematics. The sweep angle ϕ is given in degrees in the top row and the sweep time t_s in seconds is given in the bottom row of the *x*-axis. Black bars denote the flapping configuration while grey bars denote the clapping configuration.

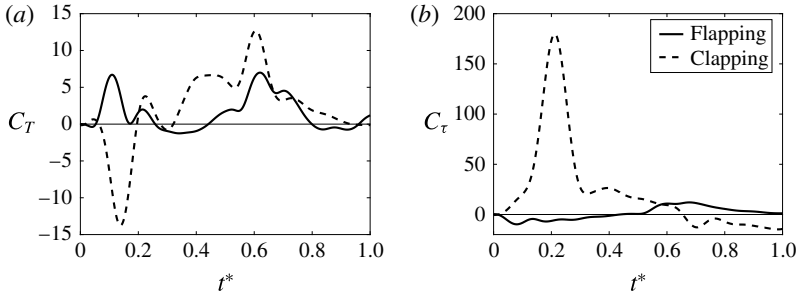


FIGURE 3. Phase averaged instantaneous C_T (*a*) and C_τ (*b*) from three trials with $\phi = 60°$ and $t_s = 2$ s. The solid black line corresponds to flapping while the dashed black line corresponds to clapping. The first half of the cycle corresponds to the opening phase of clapping while the second half of the cycle corresponds to the closing phase of clapping.

however, during the beginning of the opening phase, the area starts from zero, so the velocity must start from negative infinity. The required flow reversal from positive to negative infinity requires a large pressure gradient, which leads to an initially large torque and negative thrust seen during the first half of the cycle in figure 3. Comparison of $\overline{C}_T$ between the mechanisms for each kinematic set shows that the difference in the average thrust per cycle is small compared with the difference in the average power per cycle. It should be noted that, despite their seemingly different methods of generating thrust, the average thrust generated per cycle is remarkably similar; flapping generates a predominately positive thrust during a cycle from a vortex street, while clapping generates a positive thrust during its closing phase by creating a jet to push out fluid and a negative thrust during its opening phase by creating a low-pressure region to draw in fluid. Comparison between different kinematic sets shows that neither propulsion mechanism consistently generates more thrust. These results suggest that because the difference in $\overline{C}_T$ is small compared with

https://doi.org/10.1017/jfm.2017.252 Published online by Cambridge University Press

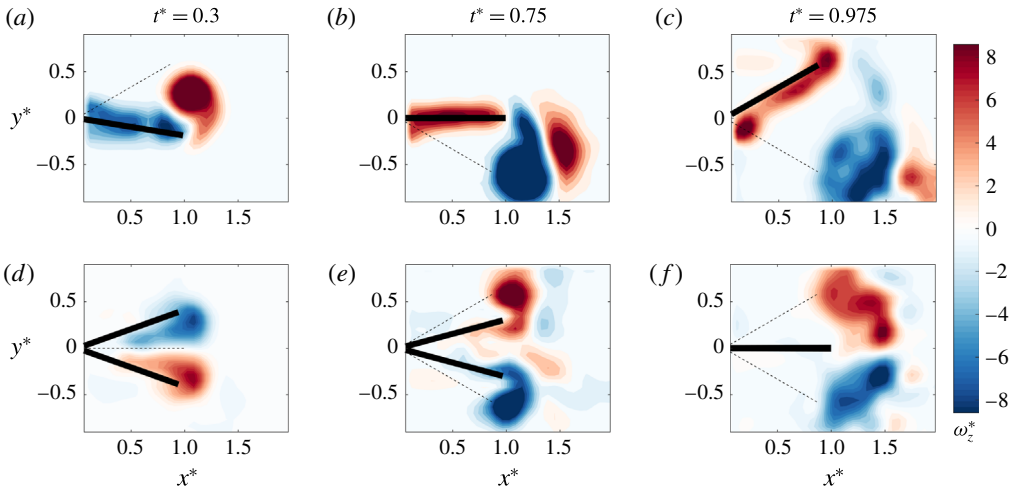


FIGURE 4. Non-dimensional vorticity contours $\omega_z^* = \omega_z/\overline{\omega}$ as a function of non-dimensional position $x^* = x/s$ and $y^* = y/L$ from PIV snapshots of flapping and clapping propulsion, shown in (*a–c*) and (*d–f*) respectively, for a 60° sweep angle and a 2 s sweep time. Panels (*a*) and (*d*), (*b*) and (*e*), and (*c*) and (*f*) correspond to snapshots taken at the same non-dimensional time $t^* = t/(2t_s)$. During the interval $0 < t^* < 0.5$, the flapping plates sweep from top to bottom while the clapping plates open outwards. During the interval $0.5 < t^* < 1$, the flapping plates sweep from bottom to top while the clapping plates close inwards. The thick black lines correspond to the locations of the plates while the thin dashed lines correspond to the original locations of the plates at the start of the half cycle.

the difference in $\overline{C}_{po}$ between the two mechanisms, and because flapping propulsion requires significantly less power than clapping propulsion, flapping propulsion is the more effective propulsion mechanism.

3.2. *Flow field investigation with DPIV*

Snapshots of the non-dimensional vorticity, $\omega_z^* = \omega_z/\overline{\omega}$, as a function of the non-dimensional position, $x^* = x/s$ and $y^* = y/L$, where $L = 2s\sin(\phi/2)$ is the excursion length of the trailing edge, at different non-dimensional times t^* are shown in figure 4 for a 60° sweep angle and a 2 s sweep time; the corresponding force and torque data are shown in figure 3. The same behaviour is exhibited for all other kinematic combinations. During each half of the cycle, the flapping plates generate a single vortex while the clapping plates generate two vortices, each which typically contains half of the circulation of a single vortex generated from flapping. Tracking of these vortices in time allows insight into their impact on the net thrust generated (figure 5) through (2.1). Here, the non-dimensional moment of vorticity, $\alpha^* = (\alpha t_s)/(1/2\ U^2 A)$, and the non-dimensional time derivative of α, $\mathrm{d}\alpha^*/\mathrm{d}t = (\mathrm{d}\alpha/\mathrm{d}t)/(1/2U^2A)$, which is used to estimate the thrust coefficient as $C_T = \mathrm{d}\alpha^*/\mathrm{d}t$, are shown as a function of t^*, allowing a straightforward comparison with the instantaneous thrust shown in figure 3. In figure 5, the solid black line denotes the sum of the contributions from all vortices, and the dotted black line, shown only for $\mathrm{d}\alpha^*/\mathrm{d}t$, denotes the mean value over the displayed time span. Data from $t^* = 0.875$ to 1 are not shown as the vortices become difficult to track. Vortices shed during the first half of the cycle are

https://doi.org/10.1017/jfm.2017.252 Published online by Cambridge University Press

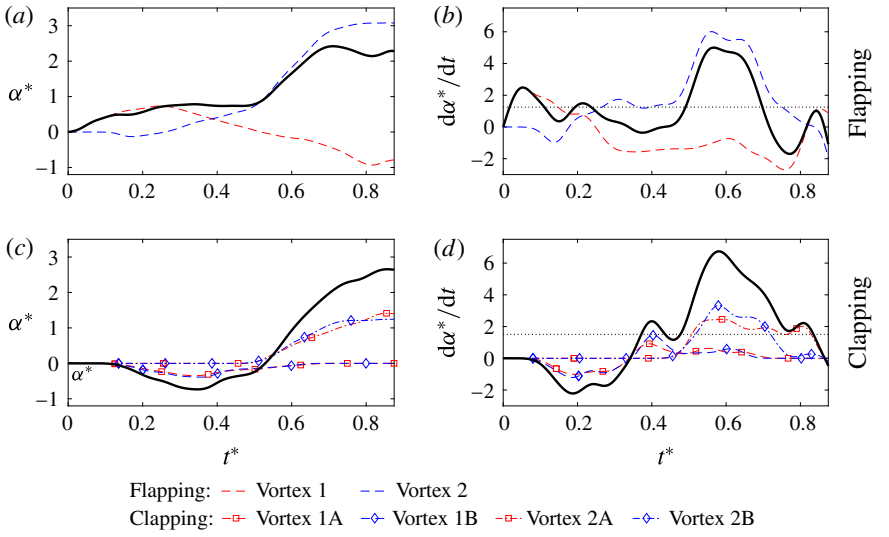


FIGURE 5. Vortex moment statistics for each vortex tracked in time from flapping and clapping propulsion in (*a*,*b*) and (*c*,*d*) respectively for a 60° sweep angle and a 2 s sweep time. The non-dimensional first moment of vorticity α^* is shown in (*a*,*c*) and the non-dimensional time derivative of α, $d\alpha^*/dt$, used as a predictor for C_T, is shown in (*b*,*d*). Vortices shed during the first half of the cycle are labelled '1' while vortices shed during the second half of the cycle are labelled '2'; if two vortices are shed during a cycle, the positive and negative vortices are labelled A and B respectively. The solid black line corresponds to the sum of the contributions from all vortices while the dashed black line, shown only for $d\alpha^*/dt$, corresponds to the mean value over the interval shown.

labelled '1' while vortices shed during the second half of the cycle are labelled '2'; if two vortices are shed during a cycle, the positive and negative vortices are labelled A and B respectively.

For flapping, during the first quarter of the cycle when the plates are accelerating, the circulation of vortex 1 increases, giving a positive contribution to the thrust. However, during the second quarter of the cycle when the plates are decelerating, the growth rate has stagnated and combined with the net drift downwards in y, noticeable by comparing the locations of vortex 1 at $t^* = 0.3$ and 0.75 in figure 4; vortex 1 gives a negative contribution to the thrust. This drift in y continues at later t^*, giving a negative contribution to the thrust during the second half of the cycle which nearly cancels the earlier positive contribution. For clapping, during the first quarter of the cycle when the plates are accelerating, the growth rates of vortices 1A and 1B increase, but here the vortices contribute negatively to the thrust because the growth rates of the vortices and their positions have opposite signs. This contribution is largely cancelled by the positive impact on the thrust generated during the second quarter of the cycle as the vortices reduce in strength and drift towards the centreline. These results imply that the main contribution to the net thrust lies in the vortex moment from the vortices generated during the second half of the cycle, which figure 5 shows to be nearly identical between the two propulsion modes. This provides an explanation for the similar thrusts seen in figure 2, as $\overline{C}_T$ predicted through vortex tracking using (2.1), $\overline{C}_T = \overline{d\alpha^*/dt}$, is 1.25 and 1.50 for flapping and clapping respectively, which is in reasonable agreement with the $\overline{C}_T$ of 1.44 and

https://doi.org/10.1017/jfm.2017.252 Published online by Cambridge University Press

2.01 for flapping and clapping respectively computed from figure 3. The discrepancy between the values is probably due to possible three-dimensionality of the flow as well as the difficulty in tracking the shed vortices as they begin to break up and diffuse; therefore, some vorticity may not be accounted for. The similarity in the net thrusts is reasonable, as the magnitudes and growth rates of the generated vortices are directly proportional to the velocity and acceleration of the plates, which are identical when comparing cases with the same overall ϕ and t_s. From the DPIV data, the circulation of a single vortex from flapping is typically twice that of a single vortex from clapping, meaning that the total circulations from the vortices are nearly identical. Furthermore, the excursions of the plates are identical when comparing cases with identical kinematics, so the vortices will grow and shed at nearly identical positions, meaning that the total α from all vortices should be similar between the two propulsion mechanisms. The drift in y can be shown to be small as vortex 2 and vortices 2A and 2B tend to primarily translate in x, noticeable by examining their positions at $t^* = 0.75$ and 0.975 in figure 4. A similar behaviour can be expected after many cycles.

3.3. *The effect of flexibility*

The effect of flexibility is investigated using polycarbonate plates of different thicknesses on a subset of the kinematic combinations. The 0.508 mm and 0.381 mm polycarbonate plates are tested with 40°, 60° and 80° sweep angles, each with a 2 s sweep time. The maximum K values for these plates are 6.549 and 2.763 respectively, meaning that large deformation occurs for all kinematic sets. The $\overline{C}_T$ and $\overline{C}_{po}$ for the 0.508 mm plates are shown in figures 6(*a*) and 6(*b*) respectively, while those for the 0.381 mm plates are shown in figures 6(*c*) and 6(*d*) respectively. The $\overline{C}_T$ for the 0.508 mm plates is similar between the two propulsion modes despite the significant deformation throughout the cycle. The $\overline{C}_{po}$ for the 0.508 mm plates shows a reduction on average in the required input power for clapping propulsion compared with that for the rigid plates; however, the input power required is on average 4.5 times greater than that for flapping propulsion. For the 0.381 mm plates, a difference between flapping and clapping becomes noticeable when comparing $\overline{C}_T$. Here, flexibility has led to a deficit in thrust for clapping propulsion, as $\overline{C}_T$ for clapping is on average 0.6 times that for flapping, probably because the plates begin to follow the flow instead of driving the flow. It should be noted that the bending rigidity for flapping propulsion is twice that of clapping propulsion, which is a likely explanation for why no significant deficit in thrust is seen in flapping propulsion. Although $\overline{C}_{po}$ for the 0.381 mm plates in clapping propulsion shows a 40 % decrease on average compared with that from the 0.508 mm plates, $\overline{C}_{po}$ is on average 2.81 times that for flapping propulsion.

The results for the 0.508 mm flexible plates suggest that an increase in flexibility will not significantly affect $\overline{C}_T$ but will significantly decrease $\overline{C}_{po}$ for clapping propulsion; the increase in flexibility provides a marginal decrease in $\overline{C}_{po}$ for flapping propulsion. A natural assumption would be that a further increase in flexibility would decrease $\overline{C}_{po}$ for clapping propulsion to the point where $\overline{C}_{po}$ would be similar between the two mechanisms but leave $\overline{C}_T$ unchanged; if this were the case, the effectivenesses of the two propulsion mechanisms would be comparable. Although the results from the 0.381 mm plates continue the trend that increasing flexibility significantly decreases $\overline{C}_{po}$ for clapping propulsion, they also show that decreasing $\overline{C}_{po}$ can decrease $\overline{C}_T$ as well, which impacts clapping more than flapping. Therefore, a further increase in flexibility will probably not make clapping propulsion more effective than flapping propulsion.

https://doi.org/10.1017/jfm.2017.252 Published online by Cambridge University Press

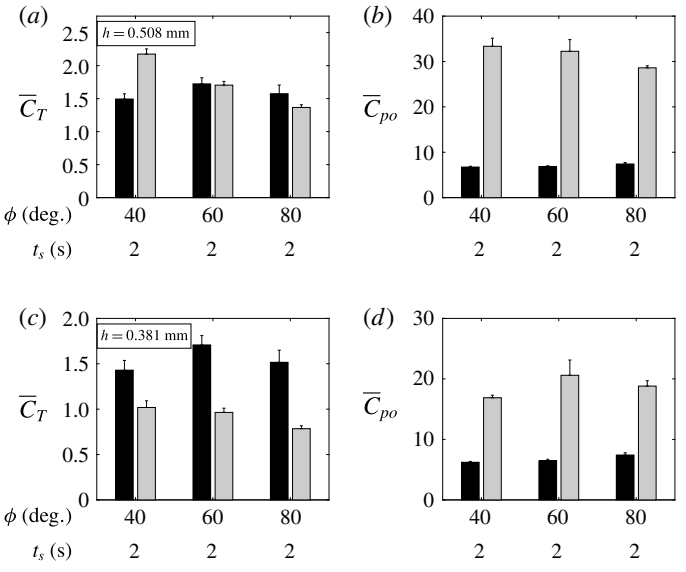


FIGURE 6. Average thrust coefficient $\overline{C}_T$ (*a*,*c*) and power coefficient $\overline{C}_{po}$ (*b*,*d*) for the flexible polycarbonate plates as a function of plate kinematics. Panels (*a*) and (*b*), and (*c*) and (*d*) correspond to the results for different flexible plates; panels (*a*) and (*c*) show the thicknesses h of the plates in the upper left corner. Black bars denote the flapping configuration while grey bars denote the clapping configuration.

3.4. *The effect of modifying the duty cycle*

The effect of modifying the duty cycle is investigated on clapping propulsion only. In clapping propulsion, the opening phase generates a negative thrust and requires a large amount of power, while the closing phase generates a positive thrust but requires less power. By modifying the duty cycle to increase the time spent (i.e. decrease the angular velocity) in the opening phase and decrease the time spent (i.e. increase the angular velocity) in the closing phase, $\overline{C}_T$ should increase and $\overline{C}_{po}$ should decrease, yielding an overall increase in effectiveness. It should be noted that modification of the duty cycle will change t_s during the opening and closing phases of a cycle but leave the total cycle time T_{cycle} unchanged. For consistency, the angular velocity in the coefficients $\overline{C}_T$ and $\overline{C}_{po}$ is defined as $\overline{\omega} = \phi/(T_{cycle}/2)$ to remain identical to that used in the previously discussed cases with the same overall kinematics. Modified duty cycles are investigated using 1.016 mm polycarbonate plates with 60° and 80° sweep angles and a 2 s sweep time. The minimum K for this plate is 12.72 at a 80° sweep angle and a 2 s sweep time, meaning that the plate is effectively rigid during all instances for the slower angular velocities. During the faster angular velocities, small deformation will occur typically at the beginning of the opening and closing phase of a cycle. Two modified duty cycles, where the opening phase took two and three times as long as the closing phase (2:1 and 3:1 duty cycles respectively), are compared with the results from an unmodified (1:1) duty cycle. The $\overline{C}_T$ and $\overline{C}_{po}$ for the 1.016 mm plates are shown in figures 7(*a*) and 7(*b*) respectively.

Modification of the duty cycle for the clapping 1.016 mm polycarbonate plates increases the $\overline{C}_T$ and decreases the $\overline{C}_{po}$ significantly. Compared with the $\overline{C}_T$ and $\overline{C}_{po}$ obtained from clapping with an unmodified duty cycle, use of a 3:1 duty cycle gives

https://doi.org/10.1017/jfm.2017.252 Published online by Cambridge University Press

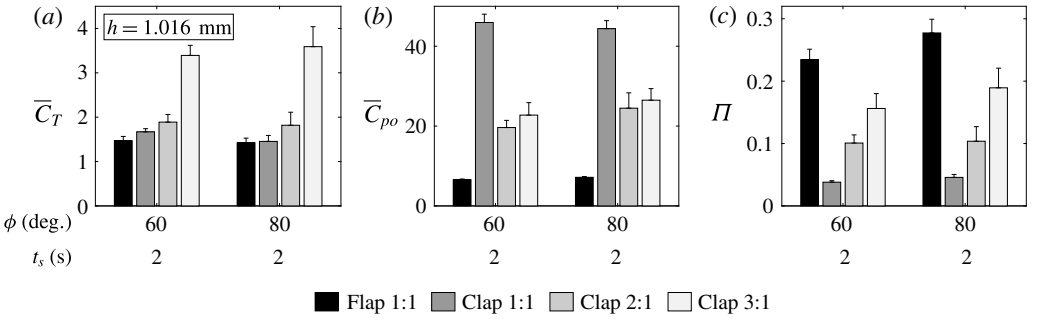


FIGURE 7. Average thrust coefficient $\overline{C}_T$ (*a*), power coefficient $\overline{C}_{po}$ (*b*) and force ratio Π (*c*) for the 1.016 mm thick polycarbonate plate as a function of the plate kinematics. Black bars denote the flapping configuration while grey bars denote the clapping configuration, with different duty cycles given as the ratio of the time spent in the opening phase to that spent in the closing phase.

a 125 % increase and a 45 % decrease respectively. Compared with the $\overline{C}_T$ and $\overline{C}_{po}$ from flapping, the $\overline{C}_T$ and $\overline{C}_{po}$ from using a 3:1 duty cycle are on average 2.42 times and 3.58 times those for flapping respectively. A simple method of comparing the effectiveness between the two propulsion mechanisms is to use the force ratio, defined as $\Pi \equiv \overline{F}/(\overline{T}/s)$, shown in figure 7(*c*). This result suggests that modification of the duty cycle for clapping propulsion causes the force ratio to approach that given by flapping propulsion. Additionally, this comparison is made with flapping propulsion without optimizing its motion; therefore, it is a reasonable assumption that the force ratio can be improved for flapping propulsion. This suggests that flapping propulsion is still the more effective mechanism, but clapping propulsion with a modified duty cycle can produce a greater thrust than flapping propulsion with an unmodified duty cycle.

4. Concluding remarks

A comparison has been made between flapping and clapping propulsion to determine which mechanism a hypothetical animal with two appendages should use. Overall, the results suggest that between *Re* of 1880 and 11 260, flapping is the more effective propulsion mechanism, but a greater thrust can be generated using clapping propulsion with a modified duty cycle compared with flapping propulsion with an unmodified duty cycle. Between the two mechanisms, the difference in the average thrust generated per cycle using the rigid aluminium plates was small compared with the difference in the average power required, for which flapping required significantly less power compared with clapping. Increase of the flexibility led to a decrease in the input power required, more so for clapping than for flapping, but did not decrease the power required enough for the effectiveness of clapping propulsion to be comparable to that from flapping propulsion. Modification of the duty cycle for rigid clapping plates led to a significant increase in the average thrust generated per cycle, which surpassed that produced during flapping propulsion, and to a significant decrease in the required power, causing the effectiveness of clapping propulsion to approach that of the unoptimized flapping propulsion. Therefore, the results suggest that if the hypothetical animal wants to use the most effective mechanism, the animal should put its two fins together and utilize a flapping motion.

https://doi.org/10.1017/jfm.2017.252 Published online by Cambridge University Press

Acknowledgements

This work was supported by the Charyk Bio-inspired Laboratory at the California Institute of Technology. N.M. and C.R. were supported by the National Science Foundation Graduate Research Fellowship under grant no. DGE-1144469. S.I. was supported by the Summer Undergraduate Research Fellowships program at the California Institute of Technology.

References

BAINBRIDGE, R. 1958 The speed of swimming of fish as related to size and to the frequency and amplitude of the tail beat. *J. Expl Biol.* **35** (1), 109–133.

COLIN, S. P., COSTELLO, J. H., KATIJA, K., SEYMOUR, J. & KIEFER, K. 2013 Propulsion in cubomedusae: mechanisms and utility. *PloS One* **8** (2), e56393.

COLIN, S. P., COSTELLO, J. H. & KORDULA, H. 2006 Upstream foraging by medusae. *Mar. Ecol.-Prog. Ser.* **327**, 143–155.

DAI, H., LUO, H., FERREIRA DE SOUSA, P. J. S. A. & DOYLE, J. F. 2012 Thrust performance of a flexible low-aspect-ratio pitching plate. *Phys. Fluids* **24** (10), 101903.

GERSHWIN, L.-A. & COLLINS, A. G. 2002 A preliminary phylogeny of pelagiidae (cnidaria, scyphozoa), with new observations of chrysaora colorata comb. nov. *J. Nat. Hist.* **36** (2), 127–148.

GRAHAM, W. M. & KROUTIL, R. M. 2001 Size-based prey selectivity and dietary shifts in the jellyfish, *aurelia aurita*. *J. Plankton Res.* **23** (1), 67–74.

HUNTER, J. R. & ZWEIFEL, J. R. 1971 Swimming speed, tail beat frequency, tail beat amplitude, and size in jack mackerel, trachurus-symmetricus, and other fishes. *Fish Bull* **69** (2), 253–266.

KIM, D., HUSSAIN, F. & GHARIB, M. 2013 Vortex dynamics of clapping plates. *J. Fluid Mech.* **714**, 5–23.

KOOCHESFAHANI, M. M. 1989 Vortical patterns in the wake of an oscillating airfoil. *AIAA J.* **27** (9), 1200–1205.

MORANDINI, A. C., DA SILVEIRA, F. L. & JARMS, G. 2004 The life cycle of chrysaora lactea eschscholtz, 1829 (cnidaria, scyphozoa) with notes on the scyphistoma stage of three other species. *Hydrobiologia* **530** (1–3), 347–354.

SAMBILAY, V. C. JR. 1990 Interrelationships between swimming speed, caudal fin aspect ratio and body length of fishes. *Fishbyte* **8** (3), 16–20.

SANE, S. P. 2003 The aerodynamics of insect flight. *J. Expl Biol.* **206** (23), 4191–4208.

WEIS-FOGH, T. 1973 Quick estimates of flight fitness in hovering animals, including novel mechanisms for lift production. *J. Expl Biol.* **59** (1), 169–230.

WILLERT, C. E. & GHARIB, M. 1991 Digital particle image velocimetry. *Exp. Fluids* **10** (4), 181–193.

WU, J. C. 1981 Theory for aerodynamic force and moment in viscous flows. *AIAA J.* **19** (4), 432–441.

YEH, P. D. & ALEXEEV, A. 2016 Effect of aspect ratio in free-swimming plunging flexible plates. *Comput. Fluids* **124**, 220–225.

https://doi.org/10.1017/jfm.2017.252 Published online by Cambridge University Press